EurJIC
European Journal of Inorganic Chemistry

Research Article
doi.org/10.1002/ejic.202400026

Chemistry Europe
European Chemical Societies Publishing

www.eurjic.org

Structure Directing Effects of the Tetraphenylphosphonium Cation upon the Formation of Lanthanoid Anilate Coordination Polymers

Carol Hua*[a]

Four lanthanoid anilate coordination polymers (CPs) were synthesised using fluoranilate and chloranilate ligands with La(III), Eu(III) and Dy(III), and PPh_4^+ as the countercation. The presence of the PPh_4^+ countercation had a structure directing effect on the CP topology, with a 3D diamondoid (dia) network obtained with La(III) whilst 2D square grid (sql) networks were obtained with Eu(III) and Dy(III). This work represents the first use of fluoranilate in lanthanoid anilate CPs. The additional hydrogen bonding sites afforded by the fluorine substituent influences the packing of the crystal structure whilst the variation in lanthanoid ion size helps determine the topology of the CP.

Introduction

Coordination polymers (CPs) and metal organic frameworks (MOFs) containing 1,4-disubstituted 2,5-dihydroxy-1,4-benzoquinone, commonly called anilic acids (H_2Xan, where X = F, Cl, Br, CN, NO_2) have been widely investigated for a range of applications including molecular magnetism,[1–21] conductivity,[9,22–24] and gas adsorption.[25–27] The appeal of using anilic acids in the synthesis of CPs stems from the ability of the ligand to exist in multiple redox states including Xan^{2-}, $Xan^{3-\bullet}$ and Xan^{4-}. The $Xan^{3-\bullet}$ state is of particular interest due the stability of the radical anion when the ligand is coordinated and potentially able to mediate electronic communication between metal centres. Iron anilate CPs have outstanding conductivity[22] and magnetic ordering[6,8,10] for porous materials due to the favourable orbital overlap between the iron and the ligand, as well as the ability of iron to exist in mixed valence states, Fe(II) and Fe(III).

The use of lanthanoid ions in anilate CPs is desirable due to the unique spectroscopic and magnetic properties of the lanthanoids. The large majority of anilate containing CPs have been synthesised with transition metals, with fewer studies dedicated to the study of lanthanoid anilate coordination polymers. The synthesis of lanthanoid CPs is more challenging due to the greater ionic nature of lanthanoids when compared to transition metals leading to larger variability of coordination environments, and the lack of predictable coordination geometries. Control over the topology of lanthanoid anilate CPs is therefore challenging to achieve. The majority of lanthanoid anilate coordination polymers are obtained as 2D (6,3)-honeycomb structures commonly containing three anilate ligands bound in a bidentate manner to the lanthanoid ion with the remaining coordination sites filled with solvent molecules such as water.[13,15,18,19,21,23,28–37] The honeycomb structures formed from lanthanoids are commonly corrugated due to the facial coordination from the solvent molecules which contrasts with the planar 2D honeycomb obtained with transition metals.[8,38] One method for obtaining predictable topologies with lanthanoid anilate coordination polymers is the use of a countercation template.[25,26,34,39] Previous studies have used tetraalkylammonium cations including Me_4N^+ and Et_4N^+ to yield 2D square grid structures[25,26,39] as well as larger aromatic cations including PPh_4^+ and 1-(diphenylmethyl)-pyridinium ($DPMP^+$) to obtain diamondoid topologies with Ce(III) and Er(III).[34] Other topologies obtained with lanthanoid anilates (some with the use of cationic templates) includes noq,[34] a mixed 2D (8,8)-(4,4)-square topology,[40] xah[41] and chiral 3D 10,3-a networks.[5]

A range of substituents on the anilate ligand have been investigated including chloranilate (Cl),[17,19,21,26,33,34,41–43] bromanilate (Br),[5,12,15,18,21,30,32] dihydroxybenzoquinone (H),[18,21,28,29] and chlorocyananilate (mixed Cl and CN).[12,23,31,37,40,44–46] Fluoranilic acid (F), however remains significantly underexplored, with the few studies using fluoranilate involving transition metal ions.[9,36,38,47–49] The use of fluoranilate may yield intriguing properties when compared to chloranilate due to the greater electron withdrawing nature of the fluorine, and its ability to form hydrogen bonds with other framework components, counterions and guest molecules within the framework voids. The smaller size of the fluorine substituent when compared to other anilate ligands (except H) may also enable the formation of novel or intriguing topologies that are otherwise not possible with the presence of larger 3,6-anilate substituents.

In this work, we aim to explore the role of the PPh_4^+ countercation in influencing the topology of lanthanoid fluoranilate and chloranilate CPs with La(III), Eu(III) and Dy(III). Given the rarity of the diamondoid topology in lanthanoid chloranilate

[a] Dr. C. Hua
School of Chemistry, The University of Melbourne, Parkville, Victoria, 3010, Australia
E-mail: carol.hua@unimelb.edu.au

Supporting information for this article is available on the WWW under https://doi.org/10.1002/ejic.202400026

Research Article
doi.org/10.1002/ejic.202400026

coordination polymers, we additionally wished to obtain diamondoid structures with other lanthanoid ions beyond Ce(III) and Er(III) from a previous study.[34] The interplay between the anilic acid substituent size with the lanthanoid ion radii on topology will be probed and the templation effects of PPh_4^+ assessed.

Results and Discussion

All coordination polymers were synthesised by layering a solution of fluoranilic acid (H_2Fan) or chloranilic acid (H_2Clan) in acetone over a solution of PPh_4Br, LiOAc and $Ln(NO_3)_3{\cdot}xH_2O$ (Ln = La, Eu, Dy) in a mixture of methanol and water (ratio 1:3) to yield $(PPh_4)[La(Fan)_2(H_2O)]$ (**1**), $(PPh_4)_2[La_2(Clan)_4(C_3H_6O)_2]\cdot 3\,C_3H_6O\cdot 4H_2O$ (**2**), $(PPh_4)[Eu(Fan)_2(CH_4O)]\cdot C_3H_6O$ (**3**) and $(PPh_4)[Dy(Fan)_2(CH_4O)]\cdot 2\,C_3H_6O$ (**4**). **1** and **3** were obtained as deep blue crystals, **2** as maroon crystals and **4** as deep green crystals. LiOAc is used in the synthesis to deprotonate the H_2Fan and H_2Clan ligands. The Fan^{2-} and $Clan^{2-}$ ligands in **1**–**4** all exist in their −2 state as indicated through the C–O and C–C bond lengths and corroborated through their FT-IR stretches (ESI, Table S4). The PPh_4^+ counterion used for charge balance is located within the voids in **1**–**4**. The bulk purity of all compounds was determined using PXRD (ESI, Figures S3-6).

Diamondoid (dia) Networks

Frameworks **1** and **2** were formed as isostructural networks featuring a diamondoid (dia) topology. The La(III) centres in **1** and **2** both exhibit a 9-c coordination environment from *O*-donors from four fluoranilate ligands binding in a bidentate manner and one acetone (**1**) or water (**2**) solvent molecule (Figure 1a and Figure S1a). Typical La(III)-O bond lengths are obtained for both **1** and **2** (ESI, Table S5). The La(III) ion contains different coordination geometries with a square antiprism for **1** and a tricapped trigonal prism for **2**. The change in coordination geometry upon changing the Fan^{2-} ligand in **1** for $Clan^{2-}$ in **2** may be attributed to the larger steric bulk imposed by the chlorine atom on the ligand when compared to the fluorine atom. **1** and **2** both exhibit an adamantane unit with minor distortion along one direction (forming a compressed hexagon) as indicated through the La-La-La angles of 90.34(1), 115.13(1) and 118.39(1)° for **1** (Figure 1b) and 100.87, 100.87, 101.78, 116.74, 119.67, 138.18° for **2** (ESI, Figure S1b).

Dr Carol Hua is currently a Senior Lecturer in the School of Chemistry, University of Melbourne. She completed her PhD in 2016 at the University of Sydney with Prof. Deanna D'Alessandro before undertaking postdoctoral positions at the University of Limerick, Ireland and Northwestern University, USA supported by the American-Australian Association and Endeavour Fellowships. Carol received a McKenzie Fellowship from the University of Melbourne in 2018 before commencing as a Lecturer at Deakin University in 2021. Carol returned to the University of Melbourne in 2023 with a research program involving the development of chiral chemical sensors and stimuli responsive materials.

The PPh_4^+ counterion occupies the void space in each of these **dia** networks featuring multiple non-covalent interactions including hydrogen bonding and π-π stacking with the anilate ligands within the coordination polymer (Figure 1c, Figure S1c). Framework **1** exhibits a close interaction of the PPh_4^+ counterion with Fan^{2-} in the framework with π-π stacking (d = 3.692 Å) between one of the phenyl rings in PPh_4^+ with a Fan^{2-} ligand, hydrogen bonding between the coordinated acetone molecule with hydrogens from the PPh_4^+ (d_{O-H} = 3.326(2) and 3.678(2) Å) and between the fluorine in the Fan^{2-} ligand with hydrogens from the PPh_4^+ (d_{F-H} = 2.950(2) and 3.709(2) Å) (Figure 1c).

Changing from Fan^{2-} to $Clan^{2-}$ in **2** results in the inclusion of acetone and water solvent molecules between the framework and the PPh_4^+ counterion within the crystal structure. The inclusion of the solvent molecule may be attributed to the lack of hydrogen bonding ability from the chlorine atom in $Clan^{2-}$ in addition to the smaller coordinated water molecule (when compared to the coordinated acetone in **1**). The water and acetone solvent molecules assist in the formation of hydrogen bonding (d_{O-H} = 3.795(4), 3.614(4), 3.749(3) Å) and CH-π interactions (d = 3.263, 3.776 Å) between the framework structure and the PPh_4^+ counterion whilst offset π-π stacking between a $Clan^{2-}$ ligand and a phenyl ring from PPh_4^+ (d = 4.145 Å) is present between the framework structure and the PPh_4^+ counterion (ESI, Figure S1c). The PPh_4^+ counterion is clearly observed within the voids of the framework structure in both **1** (Figure 1d) and **2** (ESI, Figure S1d).

No accessible void spaces are present for **1** reflecting the close packing of the framework structure with the PPh_4^+ counterion in **1**. The lack of accessible voids in **1** is reflected in the thermal gravimetric analysis (TGA) where no mass losses are observed below 180 °C (ESI, Figure S11). The first mass for **1** occurs at 208 °C with the 6% mass loss corresponding to the coordinated acetone molecule. The significantly higher temperature above the boiling point (56 °C) required to remove the acetone molecule is indicative of the tight crystal packing. A steep mass loss at 350 °C is due to decomposition of **1**.

In contrast to **1**, an accessible void space of 19.3% is present in **2** due to the inclusion of acetone and water solvent molecules within the crystal structure (ESI, Figure S12). Two stepwise mass losses are observed in the TGA, with a 5.5% mass loss between 25–80 °C due to the liberation of acetone molecules, and a 5.8% mass loss between 80–130 °C due to the loss of water molecules. The larger mass loss above 400 °C is due to decomposition of **2**.

The diamondoid topology is a relatively rare in lanthanoid anilate coordination polymers with only a handful of examples reported. Diamondoid topologies were previously obtained through templation with aromatic cations including PPh_4^+ and 1-(diphenylmethyl)-pyridinium ($DPMP^+$) together with Ce(III) and Er(III) to form $(DPMP)[Ce(Clan)_2(H_2O)]\cdot H_2O\cdot C_3H_6O$,[34]

Research Article
doi.org/10.1002/ejic.202400026

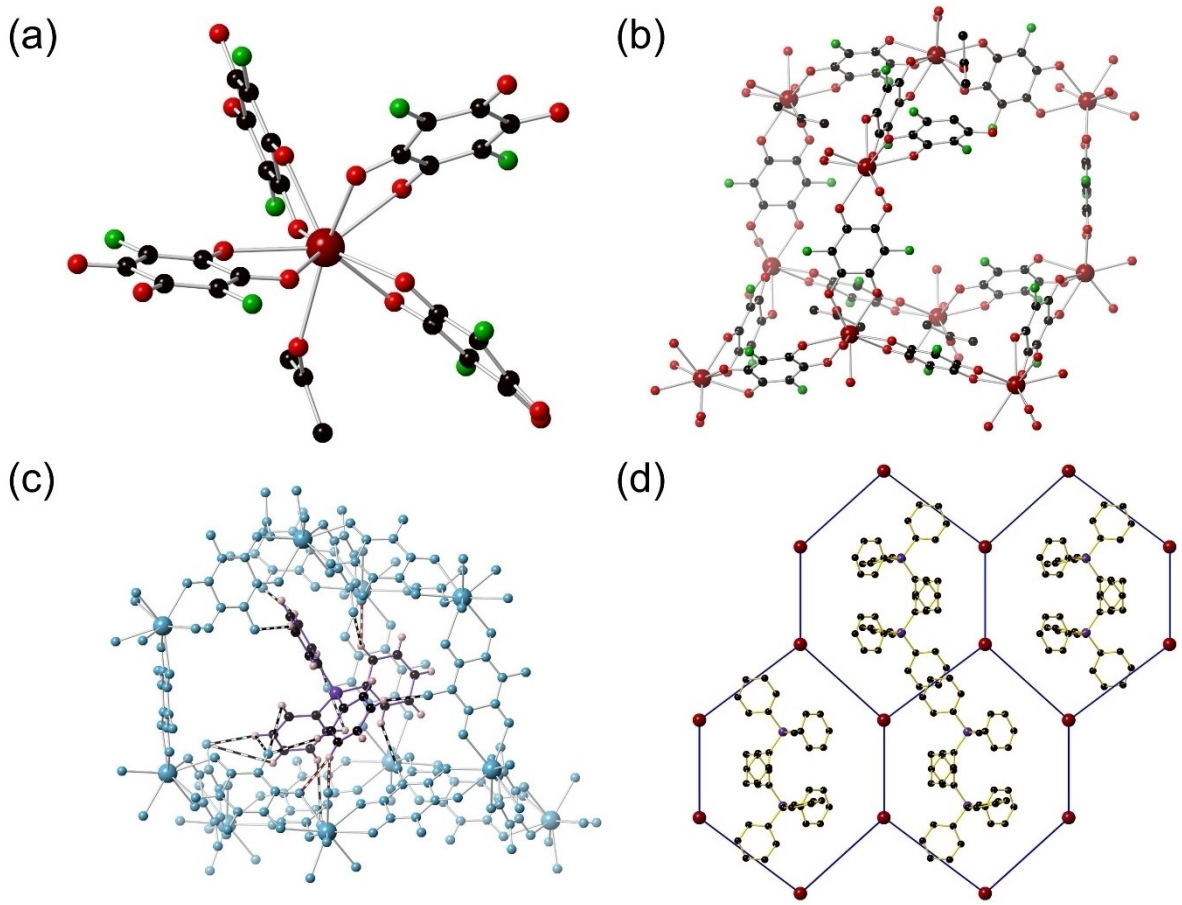

Figure 1. Structure of $(PPh_4)[La(Fan)_2(C_3H_6O)]$ **(1)** showing (a) the coordination environment around La(III), (b) the adamantane unit (without the PPh_4^+ counterion), (c) the hydrogen bonding interactions (in black and white bonds) between the PPh_4^+ counterion with the framework structure and (d) the packing of the PPh_4^+ counterions within the diamondoid topology. Colour codes for parts (a) and (b) are as follows: carbon = black, fluorine = green, oxygen = red, maroon = lanthanum. Hydrogen atoms are omitted for clarity.

$(DPMP)[Er(Clan)_2]$ and $(PPh_4)[Ce(Clan)_2(H_2O)]$.[34] The Ce(III) diamondoid networks all contained a 9-c coordination geometry containing nine *O*-donors through bidentate coordination of the $Clan^{2-}$ ligand to Ce(III) and one coordinated water molecule. The Er(III) framework contained a 8-c coordination environment with no coordinated water molecule due to the smaller ionic radius of Er(III) vs. Ce(III). The La(III) ion used in this study has a larger ionic radius than Ce(III) and it is therefore not surprising the coordination of both acetone and water solvent molecules can be accommodated on the axial position of the lanthanum ion. The influence of using aromatic cations to generate diamondoid topologies in lanthanoid anilic acid coordination polymers is further demonstrated in this study with **1** through the generation of a diamondoid topology upon changing the substituents on the anilic acid from chlorine in $Clan^{2-}$ to fluorine in Fan^{2-}. While not strictly a lanthanoid, yttrium has previously been used to obtain a diamondoid network where the oxonium ion acts as the counterion.[29]

Square Grid (Sql) Networks

Frameworks **3** and **4** were obtained as networks with a square grid (sql) topology (Figure 2, Figure S2). The Eu(III) centre in **3** and the Dy(III) centre in **4** are 9-c with a spherical capped square antiprism coordination geometry. The nine *O*-donors to the Ln(II) centres contain four Fan^{2-} ligands coordinated in a bidentate manner and one coordinated methanol solvent molecule (Figure 2a, Figure S2a). Typical Ln(III)-O bond lengths are obtained for both **3** with Eu(III)-O of 2.419(4), 2.422(5), 2.437(4), 2.445(5), 2.484(5) Å and **4** with Dy(III)-O of 2.367(3), 2.390(3), 2.397(2), 2.406(3) and 2.458(4) Å. The longer Eu(III)-O bond lengths when compared to Dy(III)-O is a reflection of the contraction in lanthanoid radii along the series. The square grids (sql) formed in **3** and **4** consist of 2D planar sheets where the sql grids display minor distortion from an ideal (90°) square with Eu–Eu-Eu bond angles of 85.28, 85.35, 91.64, 91.78° for **3** and Dy–Dy–Dy bond angles of 85.88, 86.00, 91.09, 91.37° for **4** (Figure 2b, Figure S2b).

The PPh_4^+ counterions are located in the interstitial space between the 2D sql networks resulting in a layer-to-layer distance of 11.855 Å for **3** and 13.516 Å for **4** (Figure 2c, Figure S2c). Previous sql structures obtained with $Clan^{2-}$ have

Research Article
doi.org/10.1002/ejic.202400026

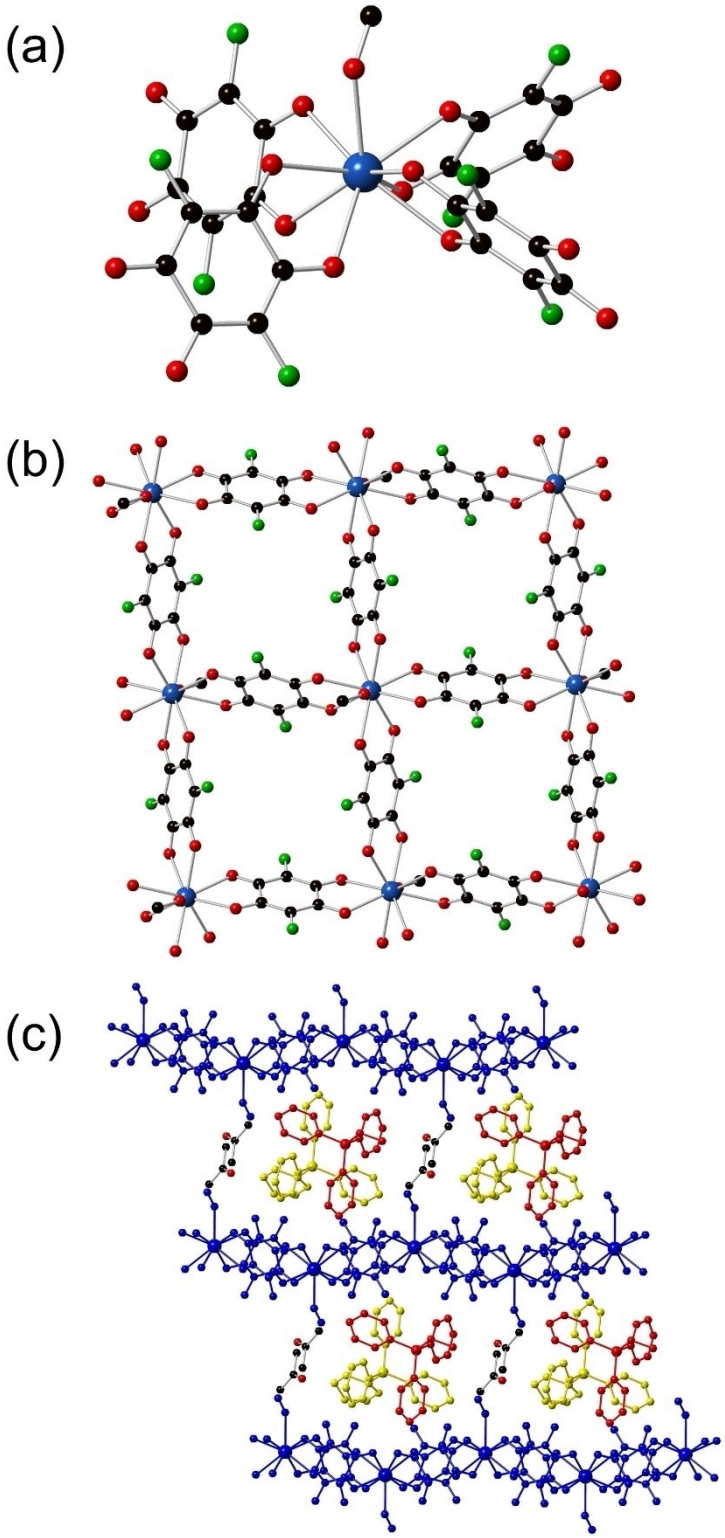

Figure 2. Structure of $(PPh_4)[Eu(Fan)_2(CH_4O)]\cdot C_3H_6O$ **(4)** showing (a) the coordination environment around the Eu(III) ion, (b) the 2D square grid sheet (without the PPh_4^+ counterions) and (c) the stacking of the 2D sheets (in blue) with the PPh_4^+ counterions (in yellow and red) located in the space between the sheets. Colour codes are as follows for parts (a) and (b): carbon = black, fluorine = green, oxygen = red, europium = blue. Hydrogens have been omitted for clarity.

predominately involved the use of Me_4N^+[26] and Et_4N^+ countercations[25,26,39] as the tetrahedral symmetry enables effective non-covalent interactions with the halogen substituents on the anilate CP, helping to template the square grid topology. The slight distortion of the square grid in **3** and **4** contrasts with previous sql grids formed using Et_4N^+ counter-

Research Article
doi.org/10.1002/ejic.202400026

ions where 90° Ln–Ln–Ln bond angles are obtained, which may be attributed to more suitable shape and orientation of Et_4N^+ over PPh_4^+.[26,39] The higher symmetry of the 2D square grids synthesised using Et_4N^+ is also reflected in the tetragonal *I*4/*mcm* or *I*4/*m* space group they crystallise in compared to the *P*-1 triclinic space group of **3** and **4**. Other sql structures have either H_3O^+[45] or $Me_2NH_2^+$[23] as the countercation. The interlayer distance is predominately influenced by the countercation that is located between the 2D layers, with larger counterions resulting in larger interlayer distances. The use of the Et_4N^+ counterion yields layer-to-layer separations of between 10.036(2) – 10.3349(2) Å, which is dependent upon the lanthanoid ion used.[26,39] The PPh_4^+ counterion therefore enables greater layer-to-layer distances of the 2D sheets to be generated, which may be advantageous for isolating the effect of through space magnetic coupling between adjacent 2D sheets. The methanol molecule coordinated on the axial position of the Ln(III) centre alternates pointing up and down along the 2D sheet but is always paired with a methanol molecule from the 2D sql sheet below such that they are facing towards each other through the interstitial space. The methanol molecules are linked through hydrogen bonding interactions with the acetone solvent molecules located within the voids of the crystal structure.

Strong hydrogen bonding interactions (**3**: $d_{F–H}$ = 3.021(7), 3.22(1), 3.46(1) Å, **4**: d_{F-H} = 3.029(5), 3.469(7), 4.070(9) Å) exist between the fluorine atom in the Fan^{2-} ligand with one of the phenyl rings of the PPh_4^+ counterion such that the phenyl ring is "sandwiched" between three Fan^{2-} ligands within the square of the sql grid (Figure 2c, Figure S2c). Hydrogen bonding interactions additionally occur between the coordinated methanol molecule and the hydrogens on the PPh_4^+ counterion (**3**: $d_{O–H}$ = 4.08(1), **4**: $d_{O–H}$ = 3.98(1) Å). Disorder of the PPh_4^+ counterion is observed in the crystal structure refinement of both **3** and **4** indicating the fluxional movement of the counterion within the voids, which contrasts with the more rigid orientation of the counterion in **1** and **2**.

Accessible void spaces are present in both **3** (21.2%) and **4** (21.7%). The similarity of the accessible void spaces is a reflection on the isostructural nature of these frameworks where the lower void space for **3** is due to the larger ionic radii of Eu(III) vs Dy(III) in **4**. The TGA of **3** (ESI, Figure S13) and **4** (ESI, Figure S14) are very similar, with a ~8% mass loss below 110 °C corresponding to the loss of the acetone solvent molecules in the crystal structure and the coordinated methanol molecule. A further mass loss is observed > 300 °C in both structures due to the decomposition of the frameworks.

Lanthanoid square grid coordination polymers containing chloranilate, bromanilate or cyanochloranilate bridging ligands have previously been reported, predominately with Me_4N^+ or Et_4N^+ counterions.[23,26,39,45] There exists a careful balance between the size of the lanthanoid ion and the substituent on the anilate ligand as to whether the lanthanoid ion will contain a coordinated solvent molecule on the axial position. The use of larger substituents such as Cl for $Clan^{2-}$ or Br in bromanilate ($Bran^{2-}$) with the late lanthanoids Gd(III) to Lu(III) resulting in 8-c lanthanoid centres with no solvent molecules coordinated. It was previously demonstrated that another type of sql grid can be formed with the early lanthanoids La(III) to Nd(III) where a solvent molecule was coordinated in the axial position, forming a 9-c coordination environment, whilst lanthanoids with slightly smaller ionic radii, Sm(III) and Eu(III) formed 8-c coordination geometries with no coordinated solvent.[39] The use of Nd(III) was demonstrated to be the "tipping point" where the 9-c Nd(III) centre could be transformed in a single crystal to single crystal transformation to an 8-c Nd(III) centre through removal of the axially coordinated water upon reduced pressure with heating. The use of the Fan^{2-} ligand containing the smaller fluorine substituents likely had an impact upon the formation of sql grids containing 9-c Eu(III) and Dy(III) lanthanoid centres given that 8-c coordination environments are formed when the larger $Clan^{2-}$ ligand is used.

The PPh_4^+ counterion as a template has enabled a degree of control over the topology in the otherwise unpredictable synthesis of lanthanoid anilate coordination polymers. The lanthanoid ion size is an important consideration as demonstrated in these results where La(III) yielded coordination polymers **1** and **2** with diamondoid topologies whilst the use of later lanthanoids with smaller ionic radii, Eu(III) and Dy(III) yielded square grids **3** and **4** respectively. The larger La(III) and longer La(III)-O bonds may better accommodate the inclusion of the PPh_4^+ counterion within the adamantane units of the diamondoid topology, being able to fully encompass the counterion through multiple non-covalent interactions. The formation of square grids in the case of Eu(III) and Dy(III) in the presence of PPh_4^+ is likely influenced by the shorter Ln(III)-O bond distances and smaller Ln(III) ionic radii, where the four-fold symmetry of PPh_4^+ aids in the formation of the sql topology. The shorter Ln(III)-O bonds may preclude the formation of the diamondoid topology due to the size of the adamantane unit that can be formed which may not be large enough to accommodate the PPh_4^+ counterion. The impact of the Ln(III) ion radius upon the formation of the diamondoid topology is supported by a previous study where the use of Er(III) was unable to form a diamondoid topology in the presence of the PPh_4^+, only yielding a (6,3)-honeycomb structure containing no counterions.[34]

Conclusions

The tetraphenylphosphonium cation has been used as a template to influence the topology in a series of lanthanoid containing fluoranilate and chloranilate coordination polymers. The use of lanthanoid ions with large ionic radii such as La(III) yielded the formation of diamondoid topologies in **1** and **2** where the PPh_4^+ counterion was located within the adamantane units enveloped by the framework structures. The use of later lanthanoids with smaller ionic radii, Eu(III) and Dy(III) yielded 2D square grids **3** and **4**, where the PPh_4^+ counterion was located in the interstitial space between the Ln(III) anilate sql grids. The use of fluoranilate in the synthesis of lanthanoid coordination polymers has yielded additional hydrogen bonding interactions with the fluorine substituent on the anilic acid.

Research Article
doi.org/10.1002/ejic.202400026

This study has demonstrated the effect of cation templation for the synthesis of predictable topologies in lanthanoid anilate coordination polymers along with the subtle interplay between the size of the anilic acid substituent and the Ln(III) ionic radius.

Experimental

All chemicals and solvents were used as obtained and without further purification. Fluoranilic acid was synthesised according to literature procedures.[50] Fourier Transform Infrared spectra were measured on a Bruker Alpha spectrometer between 4000–400 cm^{-1} with 4 cm^{-1} resolution and 32 scans and normalised as absorbance spectra. Thermal gravimetric analysis was conducted on either a Mettler Toledo TGA/SDTA851 instrument using aluminium crucibles as sample holders or a PerkinElmer TGA 8000 instrument using ceramic sample holders under high purity nitrogen. Typical analysis involved heating the sample up to 450 °C with a temperature increment of 4 °C min^{-1}. Microanalysis was carried out at the Chemical Analysis Facility – Elemental Analysis Service in the Department of Chemistry and Biomolecular Science at Macquarie University, Australia.

Single crystal X-ray diffraction data was collected on either the MX1 or MX2 beamline at the Australian Synchrotron.[51,52] In general, single crystals were transferred directly from the mother liquor into immersion oil and placed under a stream of nitrogen at 100 K. Crystal structures were solved by direct methods using the program SHELXT[53] and refined using a full matrix least-squares procedure based on F^2 (SHEXL),[54] within the Olex2[55] GUI program. In structures containing disordered solvent molecules that could not be satisfactorily modelled, the solvent mask routine within the Olex2 GUI was used.[55]

Framework Synthesis

$(PPh_4)[La(Fan)_2(H_2O)]$ (1). A solution of fluoranilic acid (9.1 mg, 0.05 mmol) in acetone (2.5 mL) was layered above a solution of $La(NO_3)_3 \cdot 6H_2O$ (10.8 mg, 0.025 mmol), PPh_4Br (52.4 mg, 0.125 mmol) and LiOAc (6.6 mg, 0.1 mmol) in a mixture of water (1.5 mL) and methanol (0.5 mL) and left to diffuse over three days. Deep blue crystals were obtained which were washed with acetone before being air dried (18.2 mg, 82 %).

$(PPh_4)_2[La_2(Clan)_4(C_3H_6O)_2] \cdot 3\ C_3H_6O \cdot 4H_2O$ (2). A solution of chloranilic acid (20.9 mg, 0.10 mmol) in acetone (5 mL) was layered above a solution of $La(NO_3)_3 \cdot 6H_2O$ (24.9 mg, 0.05 mmol), PPh_4Br (209.9 mg, 0.5 mmol) and LiOAc (13.2 mg, 0.200 mmol) in a mixture of water (3.0 mL) and methanol (1.0 mL) and left to diffuse over three days. Maroon crystals were obtained which were washed with acetone before being air dried (44.1 mg, 85 %).

$(PPh_4)[Eu(Fan)_2(CH_4O)] \cdot C_3H_6O$ (3). A solution of fluoranilic acid (9.1 mg, 0.05 mmol) in acetone (2.5 mL) was layered above a solution of $Eu(NO_3)_3 \cdot 6H_2O$ (10.7 mg, 0.025 mmol), PPh_4Br (52.4 mg, 0.125 mmol) and LiOAc (6.6 mg, 0.1 mmol) in a mixture of water (1.5 mL) and methanol (0.5 mL) and left to diffuse over three days. Deep blue crystals were obtained which were washed with acetone before being air dried (17.6 mg, 76 %).

$(PPh_4)[Dy(Fan)_2(CH_4O)] \cdot 2\ C_3H_6O$ (4). A solution of fluoranilic acid (9.1 mg, 0.05 mmol) in acetone (2.5 mL) was layered above a solution of $Dy(NO_3)_3 \cdot 6H_2O$ (8.7 mg, 0.025 mmol), PPh_4Br (52.4 mg, 0.125 mmol) and LiOAc (6.6 mg, 0.1 mmol) in a mixture of water (1.5 mL) and methanol (0.5 mL) and left to diffuse over three days. Deep green crystals were obtained which were washed with acetone before being air dried (22.2 mg, 89 %).

Electronic Supplementary Information

Crystallographic and structural details, continuous shape analysis, powder XRD, thermal gravimetric analysis and ATR-FTIR spectra. Deposition Number(s) 2325004 (for **4**), 2325005 (for **3**), 2325006 (for **1**), 2325007 (for **2**) contain(s) the supplementary crystallographic data for this paper. These data are provided free of charge by the joint Cambridge Crystallographic Data Centre and Fachinformationszentrum Karlsruhe Access Structures service.

Acknowledgements

This research was conducted by the Australian Research Council Centre of Excellence in Exciton Science (project number CE170100026) and funded by the Australian Government. This research was undertaken in part using the MX1 and MX2 beamlines at the Australian Synchrotron, part of ANSTO, and made use of the Australian Cancer Research Foundation (ACRF) detector. We acknowledge Dr Martin van Koeverden for synthetic advice and helpful discussions. Open Access publishing facilitated by The University of Melbourne, as part of the Wiley - The University of Melbourne agreement via the Council of Australian University Librarians.

Conflict of Interests

The authors declare no competing financial interest

Data Availability Statement

The data that support the findings of this study are available from the corresponding author upon reasonable request.

[1] M. Atzori, S. Benmansour, G. Mínguez Espallargas, M. Clemente-León, A. Abhervé, P. Gómez-Claramunt, E. Coronado, F. Artizzu, E. Sessini, P. Deplano, A. Serpe, M. L. Mercuri, C. J. Gómez García, *Inorg. Chem.* **2013**, *52*, 10031–10040.
[2] A. Abhervé, M. Clemente-León, E. Coronado, C. J. Gómez-García, M. Verneret, *Inorg. Chem.* **2014**, *53*, 12014–12026.
[3] A. Abhervé, S. Mañas-Valero, M. Clemente-León, E. Coronado, *Chem. Sci.* **2015**, *6*, 4665–4673.
[4] M. Atzori, F. Pop, P. Auban-Senzier, R. Clérac, E. Canadell, M. L. Mercuri, N. Avarvari, *Inorg. Chem.* **2015**, *54*, 3643–3653.
[5] S. Benmansour, C. Vallés-García, P. Gómez-Claramunt, G. Mínguez Espallargas, C. J. Gómez-García, *Inorg. Chem.* **2015**, *54*, 5410–5418.
[6] I.-R. Jeon, B. Negru, R. P. Van Duyne, T. D. Harris, *J. Am. Chem. Soc.* **2015**, *137*, 15699–15702.
[7] S. Benmansour, A. Abhervé, P. Gómez-Claramunt, C. Vallés-García, C. J. Gómez-García, *ACS Appl. Mater. Interfaces* **2017**, *9*, 26210–26218.
[8] J. A. DeGayner, I.-R. Jeon, L. Sun, M. Dincă, T. D. Harris, *J. Am. Chem. Soc.* **2017**, *139*, 4175–4184.
[9] R. Murase, B. F. Abrahams, D. M. D'Alessandro, C. G. Davies, T. A. Hudson, G. N. L. Jameson, B. Moubaraki, K. S. Murray, R. Robson, A. L. Sutton, *Inorg. Chem.* **2017**, *56*, 9025–9035.
[10] J. A. DeGayner, K. Wang, T. D. Harris, *J. Am. Chem. Soc.* **2018**, *140*, 6550–6553.
[11] L. Liu, L. Li, J. A. DeGayner, P. H. Winegar, Y. Fang, T. D. Harris, *J. Am. Chem. Soc.* **2018**, *140*, 11444–11453.

[12] A. Hernández-Paredes, C. Cerezo-Navarrete, C. J. Gómez García, S. Benmansour, *Polyhedron* **2019**, *170*, 476–485.
[13] C. Martínez-Hernández, S. Benmansour, C. J. Gómez García, *Polyhedron* **2019**, *170*, 122–131.
[14] S. Benmansour, C. J. Gómez-García, *Magnetochemistry* **2020**, *6*, 71.
[15] S. Benmansour, A. Hernández-Paredes, A. Mondal, G. López Martínez, J. Canet-Ferrer, S. Konar, C. J. Gómez-García, *Chem. Commun.* **2020**, *56*, 9862–9865.
[16] K. A. Collins, R. J. Saballos, M. S. Fataftah, D. Puggioni, J. M. Rondinelli, D. E. Freedman, *Chem. Sci.* **2020**, *11*, 5922–5928.
[17] A. Mondal, S. Roy, S. Konar, *Chem. Eur. J.* **2020**, *26*, 8774–8783.
[18] S. Benmansour, A. Hernández-Paredes, M. Bayona-Andrés, C. J. Gómez-García, *Molecules* **2021**, *26*, 1190.
[19] S. Benmansour, C. J. Gómez-García, A. Hernández-Paredes, *Crystals* **2022**, *12*, 261.
[20] L. Wang, R. J. Papoular, N. E. Horwitz, J. Xie, A. Sarkar, D. Campisi, N. Zhao, B. Cheng, G. L. Grocke, T. Ma, A. S. Filatov, L. Gagliardi, J. S. Anderson, *Angew. Chem. Int. Ed.* **2022**, *61*, e202207834.
[21] S. Benmansour, C. Pintado-Zaldo, J. Martínez-Ponce, A. Hernández-Paredes, A. Valero-Martínez, M. Gómez-Benmansour, C. J. Gómez-García, *Cryst. Growth Des.* **2023**, *23*, 1269–1280.
[22] L. E. Darago, M. L. Aubrey, C. J. Yu, M. I. Gonzalez, J. R. Long, *J. Am. Chem. Soc.* **2015**, *137*, 15703–15711.
[23] S. A. Sahadevan, N. Monni, A. Abhervé, G. Cosquer, M. Oggianu, G. Ennas, M. Yamashita, N. Avarvari, M. L. Mercuri, *Inorg. Chem.* **2019**, *58*, 13988–13998.
[24] M. L. Mercuri, F. Congiu, G. Concas, S. A. Sahadevan, *Magnetochemistry* **2017**, *3*, 17.
[25] B. F. Abrahams, M. J. Grannas, T. A. Hudson, S. A. Hughes, N. H. Pranoto, R. Robson, *Dalton Trans.* **2011**, *40*, 12242–12247.
[26] C. J. Kingsbury, B. F. Abrahams, J. E. Auckett, H. Chevreau, A. D. Dharma, S. Duyker, Q. He, C. Hua, T. A. Hudson, K. S. Murray, W. Phonsri, V. K. Peterson, R. Robson, K. F. White, *Chem. Eur. J.* **2019**, *25*, 5222–5234.
[27] Y. Lin, L. Yu, S. Ullah, X. Li, H. Wang, Q. Xia, T. Thonhauser, J. Li, *Angew. Chem. Int. Ed.* **2022**, *61*, e202214060.
[28] B. F. Abrahams, J. Coleiro, B. F. Hoskins, R. Robson, *Chem. Commun.* **1996**, *1996*, 603–604.
[29] B. F. Abrahams, J. Coleiro, K. Ha, B. F. Hoskins, S. D. Orchard, R. Robson, *J. Chem. Soc. Dalton Trans.* **2002**, *2002*, 1586–1594.
[30] S. Benmansour, I. Pérez-Herráez, G. López-Martínez, C. J. Gómez García, *Polyhedron* **2017**, *135*, 17–25.
[31] S. Benmansour, A. Hernández-Paredes, C. J. Gómez-García, *Magnetochemistry* **2018**, *4*, 58.
[32] S. Benmansour, A. Hernández-Paredes, C. J. Gómez-García, *J. Coord. Chem.* **2018**, *71*, 845–863.
[33] S. Benmansour, I. Pérez-Herráez, C. Cerezo-Navarrete, G. López-Martínez, C. Martínez Hernández, C. J. Gómez-García, *Dalton Trans.* **2018**, *47*, 6729–6741.
[34] K. Bondaruk, C. Hua, *Cryst. Growth Des.* **2019**, *19*, 3338–3347.
[35] N. Monni, J. J. Baldoví, V. García-López, M. Oggianu, E. Cadoni, F. Quochi, M. Clemente-León, M. L. Mercuri, E. Coronado, *Chem. Sci.* **2022**, *13*, 7419–7428.
[36] M. P. van Koeverden, B. F. Abrahams, C. Hua, T. A. Hudson, R. Robson, *Cryst. Growth Des.* **2022**, *22*, 1319–1332.
[37] M. Oggianu, A. Abhervé, D. Marongiu, F. Quochi, J. R. Galán-Mascarós, F. Bertolotti, N. Masciocchi, N. Avarvari, M. L. Mercuri, *Crystals* **2023**, *28*, 763.
[38] C. J. Kingsbury, B. F. Abrahams, D. M. D'Alessandro, T. A. Hudson, R. Murase, R. Robson, K. F. White, *Cryst. Growth Des.* **2017**, *17*, 1465–1470.
[39] C. Hua, H. M. Tay, Q. He, T. D. Harris, *Aust. J. Chem.* **2019**, *72*, 778–785.
[40] F. Artizzu, M. Atzori, J. Liu, D. Mara, K. Van Hecke, R. Van Deun, *J. Mater. Chem. C* **2019**, *7*, 11207–11214.
[41] O. Y. Trofimova, A. V. Maleeva, I. V. Ershova, A. V. Cherkasov, G. K. Fukin, R. R. Aysin, K. A. Kovalenko, A. V. Piskunov, *Molecules* **2021**, *26*, 2486.
[42] P. E. Riley, S. F. Haddad, K. N. Raymond, *Inorg. Chem.* **1983**, *22*, 3090–3096.
[43] C. Robl, *Mater. Res. Bull.* **1987**, *22*, 1483–1491.
[44] S. Ashoka Sahadevan, F. Manna, A. Abhervé, M. Oggianu, N. Monni, V. Mameli, D. Marongiu, F. Quochi, F. Gendron, B. Le Guennic, N. Avarvari, M. L. Mercuri, *Inorg. Chem.* **2021**, *60*, 17765–17774.
[45] P. Gómez-Claramunt, S. Benmansour, A. Hernández-Paredes, C. Cerezo-Navarrete, C. Rodríguez-Fernández, J. Canet-Ferrer, A. Cantarero, C. Gómez-García, *Magnetochemistry* **2018**, *4*, 6.
[46] M. Oggianu, F. Manna, S. Ashoka Sahadevan, N. Avarvari, A. Abhervé, M. L. Mercuri, *Crystals* **2022**, *12*, 763.
[47] R. Murase, C. J. Commons, T. A. Hudson, G. N. L. Jameson, C. D. Ling, K. S. Murray, W. Phonsri, R. Robson, Q. Xia, B. F. Abrahams, D. M. D'Alessandro, *Inorg. Chem.* **2020**, *59*, 3619–3630.
[48] Y. Sekine, J. Chen, N. Eguchi, H. Miyasaka, *Chem. Commun.* **2020**, *56*, 10867–10870.
[49] K. M. Clutterbuck, B. F. Abrahams, T. A. Hudson, M. P. van Koeverden, *Dalton Trans.* **2022**, *51*, 9199–9205.
[50] K. Wallenfels, K. Friedrich, *Chem. Ber.* **1960**, *93*, 3070–3082.
[51] T. M. McPhillips, S. E. McPhillips, H. J. Chiu, A. E. Cohen, A. M. Deacon, P. J. Ellis, E. Garman, A. Gonzalez, N. K. Sauter, R. P. Phizackerley, S. M. Soltis, P. Kuhn, *J. Synchrotron Radiat.* **2002**, *9*, 401–406.
[52] D. Aragao, J. Aishima, H. Cherukuvada, R. Clarken, M. Clift, N. P. Cowieson, D. J. Ericsson, C. L. Gee, S. Macedo, N. Mudie, S. Panjikar, J. R. Price, A. Riboldi-Tunnicliffe, R. Rostan, R. Williamson, T. T. Caradoc-Davies, *J. Synchrotron Radiat.* **2018**, *25*, 885–891.
[53] G. Sheldrick, *Acta Crystallogr. Sect. A* **2015**, *71*, 3–8.
[54] G. Sheldrick, *Acta Crystallogr. Sect. C* **2015**, *71*, 3–8.
[55] O. V. Dolomanov, L. J. Bourhis, R. J. Gildea, J. A. K. Howard, H. Puschmann, *J. Appl. Crystallogr.* **2009**, *42*, 339–341.

Manuscript received: January 15, 2024
Revised manuscript received: May 15, 2024
Accepted manuscript online: May 15, 2024
Version of record online: July 19, 2024